

Vulnerability on base-isolated buildings and horizontal directionality in Peru

Este documento se centra en el diseño de desplazamientos dirigidos al riesgo sísmico para edificios con aislamiento sísmico en Perú.

El objetivo principal es determinar los desplazamientos de diseño para edificios con base aislada, especialmente en hospitales de concreto armado de cuatro pisos en zonas de alta sismicidad (Z4), y con suelos intermedios (S2).

El estudio subraya la importancia del uso de sistemas de aislamiento sísmico en edificaciones críticas como hospitales en zonas de alta sismicidad, asegurando que el diseño mantenga un riesgo de

Arnold Mendo
arnold.mendo@pucp.pe
15 de diciembre de 2024

colapso extremadamente bajo en caso de terremotos severos.

Se muestra la importancia de la inclusión de la direccionalidad espectral en la estimación de la vulnerabilidad estructural de sistemas con estructuras sísmicas aisladas.

https://doc.uni75paime.org/Seismic_Risk_Targeted_in_Peru.pdf

Arnold Mendo
arnold.mendo@pucp.pe

Citar: J. PAIME, 2025, 2, 29-62
15 de diciembre de 2024

Seismic Risk-Targeted Displacements Design for seismically isolated building in Peru

Arnold R. Mendo ¹

Abstract The final goal of this work is to determine the design displacements for base-isolated buildings in Peru with a seismic risk-target that requires the integration of seismic hazard curves and fragility function. The fragility functions are obtained for a typical hospital corresponding to four stories reinforced concrete isolated-building. The case of study was located in the highest seismic region (Z4) for intermediate type soil. The collapse fragility functions were derived through incremental dynamic analysis considering different sources of aleatory and epistemic uncertainties. In particular, the effects of record-to-record and model variability have been investigated. The seismic hazard curves were obtained from a study carried out in eleven cities of the Peruvian territory located in zone Z4, for intermediate soil, and soft soil. The directional effects of the ground motion of two horizontal components on the hazard curve were approximate by the amplification of the seismic hazard curves through the ratios of the maximum-direction spectral displacements and the geometric mean. The directionality ratios were obtained from a set of 198 acceleration seismic records measured during 40 earthquakes events belongs to the Peruvian database grouped into three types of soil: hard soil (S1), intermediate soil (S2), and soft soil (S3), according to the Peruvian seismic codes E.030 and E.031. The study shows that the directionality factor for the considered signals has an average value equal to 1.30. Furthermore, it's found the probability of a collapse was 0.002%, much less than the limit established by ASCE SEI7-16 of 2.5%.

Keywords · Seismic isolation system · Risk target Risk · Two horizontal components · Code design spectrum · Seismicity · Time history response analysis · Seismic incident angle · Fragility curves

1 Introduction

Seismic base isolation is one of the popular seismic protection systems means of seismic hazard mitigation. Their most important feature of this system is that its increased flexibility increases the natural vibration period of the structure (usually between 2.5 s to 3.5 s), decoupling the structure from the ground to absorb the earthquake energy, thereby reducing the energy transferred to the structure.

Seismic base isolation is one of the popular seismic protection systems means of seismic hazard mitigation. Their most important feature of this system is that its increased flexibility increases the natural vibration period of the structure (usually between 2.5 s to 3.5 s), decoupling the structure from the ground to absorb the earthquake energy, thereby

□ Arnold R. Mendo. arnold.mendo@pucp.pe

¹ Ph.D. (c) Civil Engineering Department, Pontifical Catholic University of Peru, Lima, Peru.

reducing the energy transferred to the structure.

The increasing use of seismic isolation in Peru being in recent years since the Peruvian Seismic Code E.030 has been recently updated in January of 2018 (SENCICO, 2018). It has established that the health facilities of the second and third level (according to the regulations of the Ministry of Health) located in the regions of greatest seismic danger (zones 4 and 3), must be designed with seismic base isolation systems (BIS). Also, in December 2018 was published the Peruvian design code of Seismic Isolation (SENCICO, 2019).

This code has adopted several requirements for base isolation provisions of ASCE 7 Standard developed for foreign seismic conditions that may not accurately represent the Peruvian seismicity (Mendo, 2015; Mendo and Fernandez-Davila, 2017, 2018; Fernandez-Davila and Mendo, 2020).

For the United States Luco et al. (2007) proposed a new approach “risk-targeted maximum considered earthquake” (MCE_R), that targets a constant risk level across that country (ASCE/SEI4-16, 2016; Luco et al., 2007). They find that the 2003 NEHRP seismic ground motion design led to non-uniform risk across US territory. By targeting the average collapse probability in 50 years, which they found to be around 1%, Luco et al. (2007) calculated new seismic ground motion design maps with ratios between 0.7 to 1.15 concerning the 2003’s proposal. Hence, the probability of structural collapse is of paramount concern such as explained by Luco et al. (2007).

The goal of a uniform risk of collapse has enough advantages over the uniform hazard, although with some pending problems, such as the difficulty of trying to define what risk is “acceptable”. Targeting a non-zero value of collapse risk accepts that some buildings will collapse during earthquakes, even when they were designed following the current building code, potentially leading to human casualties. Another problem may be the need to derive the fragility curves for a wide variety of designed structures according to the codes with different geometries and materials and with two relevant issues concerning the used fragility functions, such as: what value of the standard deviation (β) in the fragility curve may be used? and, indeed, whether the lognormal distribution should continue to be used?. Other outstanding issues and gave some possible solutions were discussed by Douglas and Gkimprxis (2017, 2018).

The difference between uniform-hazard and uniform-risk maps depends on the convolution of the shape of the ground motion versus the annual frequency of exceedance curve (hazard curve), and the structural sensitivity (vulnerability of collapse) to ground motion “fragility function” (Judd and Charney, 2014; Luco et al., 2007; Luco and Kircher, 2007). The calculation of risk requires the integration of seismic hazard curves and structural vulnerability.

The risk-targeted MCE_R maps also incorporate the maximum direction ground motions. The maps were developed by the Building Seismic Safety Council in collaboration with the U.S. Geological Survey (USGS), two of the international agencies that participate in the National Earthquake Hazards Reduction Program (NEHRP), and were adopted into the 2010 edition of the American Society of Civil Engineers (ASCE) Standard ASCE/SEI 7–10, Minimum Design Loads for Buildings and Other Structures, and subsequently into the ASCE/SEI 7-16 (ASCE/SEI7-10, 2010; ASCE/SEI7-16, 2016; FEMA 451, 2006).

The reason for use of the maximum direction of the ground motions (MD) is because many engineers find the MD to be a very meaningful parameter for structural design. In general, the structures can fail due to the seismic action represented for the two horizontal acceleration components acting simultaneously in the most unfavorable direction measured through to the orientation of the in-plan seismic incident angle (Fernandez-

Davila, 2007). However, for structures that have similar behavior in multiple directions, such as the isolated structures with similar strength and stiffness in both directions, it is reasonable to consider that the maximum acceleration component rotated of ground motion controls its collapse (Stewart et al., 2011; Watson-Lamprey, 2010). The unconservative bias in collapse capacity was simplified in the ground motion map (ASCE 7-10) and increases the USGS geomean uniform-hazard spectral accelerations to approximate MD demand. The approximation is based on the ratio of MD to geomean spectral demand. For far-field seismic ground motions in the western United States, the median ratio was 1.20 and 1.27, for spectral accelerations evaluated in periods equal to 0.2-second and 1.0-second, respectively. In the central and eastern United States, these ratios were 1.28 and 1.35 (Judd and Charney, 2014). The MD spectral acceleration is determined by calculating the maximum spectral acceleration based on both horizontal components for an entire orbit (seismic incident angle evaluated from 0° to 360°). The MD is the orientation of the seismic incident angle with the maximum spectral demand, identified by the orbital point farthest from the origin of the coordinates.

The structural vulnerability of an element under some levels of ground motion intensity measure (IMs), will result in the development of a seismic fragility function. The concept of a fragility function in earthquake engineering dates at least to Kennedy et al. (1980), who define a fragility function as a probabilistic relationship between frequency of failure of a structural element of a nuclear power plant and PGA. A more general definition would be, that the fragility function is a mathematical function that expresses the probability that some undesirable event occurs as a function of some measure of the environmental excitation (typically a measure of acceleration, deformation, or force during an earthquake). Another definition is that the fragility function represents the cumulative distribution function of the capacity of a structural element to resist an undesirable limit state (Porter, 2017). Typically, the assessment of collapse capacity in terms of the fragility function, is based on time history nonlinear earthquake response analysis (THNERA), either incremental dynamic analysis (IDA), Cloud analysis, or multi-stripe dynamic analysis using a set of acceleration records of seismic ground motions (Cardone et al., 2019).

A variety of approaches can be used to study the effects of modeling uncertainties on the seismic performance of structures. Several researchers have proposed applying THNERA combined with Monte Carlo simulation to quantify the uncertainty for structural models with nondeterministic parameters (Beheshti-Aval et al., 2014; Choi, 2008).

Ibarra (2003) proposed a method to propagate the uncertainty from model parameters to structural behavior using first-order-second-moment (FOSM) principles verified through Monte Carlo to evaluate the collapse capacity uncertainty. As a performance improvement, Latin Hypercube Sampling (LHS) (McKay et al. 1979) has also been proposed instead of classic random sampling. Kazantzi et al. (2008) used Monte Carlo with LHS to incorporate uncertainty into steel frame fragility curves. Liel et al. (2009) used IDA with Monte Carlo and FOSM coupled with a response surface approximation method to evaluate the collapse uncertainty of a reinforced-concrete building. On a similar track, Dolsek (2009) and Vamvatsikos & Fragiadakis (2010) have proposed using Monte Carlo with efficient Latin Hypercube Sampling (LHS) on IDA to achieve the same goal (Vamvatsikos, 2014).

Many investigations have been done on developing fragility function for each structure type especially for base-isolated highway bridges and in less quantity for base-isolated buildings. For example, the work carried out by Bakhshi and Mostafavi (2014) development of fragility curves for base-isolated of reinforced concrete moment-resisting

frames. They consider three 2-D structures for 3, 7, and 12 stories, using Lead Rubber Bearing (LRB) and sets of 7 records including near-fault and far-field. They concluded, that although near-fault earthquakes have a high vulnerability on fixed base buildings, their effects on base-isolated are more. Mansouri et al. (2017), estimated seismic fragility function of LRB Base Isolated Frames Using Performance-Based Design. They evaluated the seismic performance of base-isolated structures with lead-rubber bearing (LRB) using IDA analysis for 3- and 9-story buildings using 22 earthquake records which were far-fault. Their results show that, with the increasing design period of the isolator, the amount of failure probability is decreased rather than the isolator with the smaller design period. Cardone et al. (2019) developing collapse fragility curves for base-isolated buildings through incremental dynamic analysis. The set of collapse fragility functions was derived for existing reinforced concrete-frame buildings, designed for gravity loads only and then retrofitted with rubber-based and friction-based isolation systems. They did some comments on the possible use of the results of this study for practical applications. Donatello et.al (2017) has been chosen the FOSM approach to propagate structural uncertainties and quantify their effect on the collapse fragility of base-isolated structures. They consider the basic assumption of FOSM that is that each random variable linearly affects the collapse capacity of the structure and it may be critical when the limit state functions are highly nonlinear and are not the case of base-isolated buildings, whose “effective” fundamental period does not elongate significantly before structural collapse (Cardone et al., 2019).

Besides, base isolation provisions in ASCE/SEI 7 Standard have been historically shown to be conservative in estimating seismic demands and may have unacceptable probabilities of collapse in the MCE_R . The reason for this behavior is an inappropriate combination of strength in the superstructure and isolator displacement capacity (Hassan, 2020; Kitayama and Constantinou, 2018, 2019). An acceptable probability of collapse in the MCE_R for seismically isolated buildings designed by criteria of ASCE/SEI 7 is achieved when the isolator displacement capacity and the strength of the superstructure are increased. When the response modification coefficient R is reduced to unity, the displacement capacity of the isolators is increased to $1.5DM$, where DM is the displacement demand in the MCE_R , and stiffening behavior is provided beyond this displacement limit, an enhanced collapse performance is achieved (Kitayama and Constantinou, 2019). Although there are several questions to the risk-targeting approach, such as those described by (Douglas and Gkimprixis, 2017, 2018), there is a tendency to calculate the acceleration to design of seismic isolation system with a seismic risk-target in the MCE_R .

Current seismic Peruvian building codes E.030 and E.031 are based on results from a probabilistic seismic hazard analysis (PSHA). The peak ground acceleration (PGA) is used to calculate the displacements of the design of buildings with seismic isolation with the same probability of being exceeded in a given year in any area with the same PGA value.

The annual probability that defines PGA in the E.030 code is $1/475=0.0021$ (10% in 50 years or a return period of 475 years assuming a Poisson process). The PGA defined in the E.031 code for the maximum possible earthquake is 1.5 times the PGA value defined in code E.030. For isolated buildings designed with the Peruvian code E.031, with the maximum displacement in PGA of the PSHA, the question arises, whether the isolation system will have adequate performance controlling the peak story drift, residual story drift, and floor accelerations.

The effect of directionality and site response on uniform-hazard ground motion hazard of the Peruvian code E.030 is based on the geometric mean (“geomean”) of two horizontal

components, because that description is embedded in the ground motion attenuation models (Atkinson and Boore, 2003; Sadigh et al., 1997; SENCICO, 2017; Young et al., 1997; Zhao et al., 2006). In Peru, the first study to estimate the MD factors was conducted by Mendo (2015) and Mendo and Fernandez-Davila (2016, 2018, 2018) using 28 earthquake acceleration time histories from 14 earthquake events of the Peruvian database. The average calculated values were 1.32 and 1.24 for longer and shorter periods 1.0 s, respectively (Mendo, 2015; Mendo and Fernandez-Davila, 2016, 2017, 2018).

In this work, the fragility curves are developed for a structure located in zone 4 (high seismicity) in soil type S2 (shear wave velocities between 350 m/s and 550 m/s), considering the effect of directionality through the MD factor. These curves are developed to calculate the design displacements of buildings with seismic isolation in Peru with a seismic risk target of the next paper.

2 Current Practice of isolated-structures in Peru

The use of passive protection systems, such as BIS, provides an alternative to the traditional ductile design, preventing damage and keeping the structure fully operational during and after a major earthquake. In Peru, an increase in the number of BIS in recent years there has been, since the Peruvian Ministry of Health and the Peruvian Seismic Code E.030 (SENCICO, 2016), have disposed of that all hospital buildings in seismic zones 4 and 3 (zones with the higher seismic hazard), must be isolated-buildings.

For other buildings such as ports, airports, communication centers, firemen and police buildings, schools, public buildings for important document records, and files, the use of BIS is not compulsory but there is a great interest in your use.

Recently in December 2018 was published the Peruvian design code of Seismic Isolation that establishes the minimum requirements for the design of BIS in Peru (SENCICO, 2019). Before this publication, the Peruvian code for earthquake-resistant design of buildings with a fixed base E.030, in its 2016 update, established that health buildings (public and private) of the second and third levels, as regulated by the Ministry of Health, located in zones 4 and 3, should use seismic isolation systems. The Peruvian code E.030 clarified that the use of BIS or energy dissipation systems was allowed in the building, provided that the provisions of that code (minimum shear force at the base and maximum drift), and as applicable the requirements of the American code "Minimum Design Loads for Building and Other Structures", ASCE/SEI 7-10, Structural Engineering Institute of the American Society of Civil Engineers (SENCICO, 2016).

The common practice for the design of Peruvian isolated-buildings before the publication of the Peruvian code E.031 consisted of controlling the drift and accelerations for two levels of seismic inputs, according to the seismic design (SD) and the seismic maximum probable (SMP). The SD was obtained for a spectral acceleration with a 10% probability exceedance in 50 years ($T_r = 450$ years) and was used to ensure that the superstructure remains in the elastic range. The SMP was calculated as 1.5·SD (approximately 2% probability of exceedance in 50 years - $T_r = 2475$ years) and was used to verify the deformations of the isolation system and the systems that cross the interface of isolation. The design of the isolation system for the SD consisted of controlling the floor drift at maximum values of 2 ‰ and 3 ‰ and the maximum absolute acceleration of the floor at values of 0.2·g and 0.3·g, for the analysis of spectral response and time history, respectively.

Furthermore, it was common practice to restrict the critical damping for the SD, between 15% and 25%, to control the displacements and accelerations of the structural system.

Peru has also increased the number of seismically isolated structures in recent years:

50% corresponds to hospital buildings and 50% corresponds to university buildings, offices, and housing buildings and there are isolated-buildings of up to 17 levels. In seismic zone 4 (zone with the greater seismic hazard), without torsional effects and damping of 20%, the seismic joint on average is less than 400 mm between the isolated and non-isolated parts. In seismic zone 3 (intermediate seismic hazard), the seismic joint could be less than 300 mm, and for seismic zone 2 (zone with less seismic hazard), it could be less than 250 mm.

Since 2019, standard E.031 establishes the requirements for the design of isolated-buildings in Peru. This code establishes that the drift limits are 0.0035 and 0.0050 when using the spectral response and time history methods, respectively. It is important to mention that this code only considers the calculation of a single level of seismic demand for the so-called maximum earthquake considered (MEC). This level of seismic demand is obtained by amplifying the spectral acceleration of the Peruvian code E.030 (fixed base), by a factor of 1.5. The spectral acceleration of the Peruvian code is calculated for a 10% probability of exceedance ($T_r = 475$ years), therefore, the spectral acceleration for the MEC, approximately corresponds to the spectral acceleration for a 2% probability of exceedance in 50 years. ($T_r = 2475$ years).

The BIS is mainly based on elastomeric isolators with and without lead core and in a smaller quantity frictional pendulum and the current design practice shown a combination of elastomeric isolators and friction sliders.

Otherwise, the required investment in the building structure for a BIS represents around the US \$30 or \$50 per square meter which can be high, compared to other countries, because there is no local production yet. Although there are some structural labs in Peru, they still are not able to perform such tests. Also in the country, there are not still laboratories to develop the tests required by seismic isolation systems, the reason for which the tests are carried out in foreign countries (Speicher et al., 2017).

3 Seismic Hazard Ground Motion

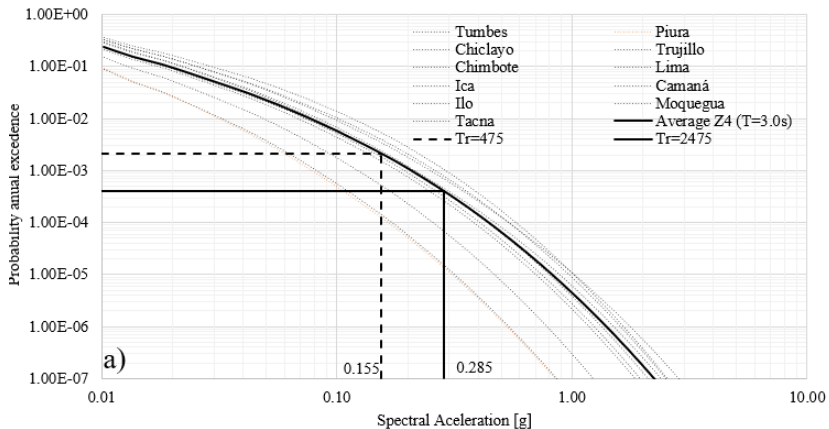
Peru is strongly affected by a subduction mechanism. Along the South American margin, the Nazca plate subducts beneath the South American plate, a zone where many severe earthquakes with moment magnitude $M_w > 7.5$, which have caused thousands of deaths and large economic losses. The major earthquake disaster in Peru of 1970 occurred in the region of Ancash, about 400 km north of Lima. Due to the high vulnerability of the adobe and unreinforced masonry constructions, there were more than 70,000 deaths and several cities destroyed. The majority of these victims were the result of a mud flood that buried the town of Yungay in the Andes highlands. In recent years, the destruction caused by medium earthquakes of 2001 and 2007 has been reported.

Villegas-Lanza et al. (2016) conducted a study for the entire coastal edge of Peru using GPS information collected until 2015 determining the main areas of maximum seismic coupling or roughness on the friction surface between the Nazca and South American plates. In front of the coasts of central and southern Peru, the displacement to be produced and the energy to be released could give rise to an earthquake with an $M_w > 7.5$, similar to that occurred in front of the coastal zone of the city of Concepción (Chile) in the year 2010 (Tavera, 2017). This confirms that Seismic risk is high in Peru. Also, the recent important earthquakes that occurred in Peru such as Atico, Arequipa in 2001 (M_w 8.4), and Pisco, Ica in 2007 (M_w 8.0), motivated the updating and incorporating of new provisions in Peruvian Seismic Code E.030 (SENCICO, 2018).

Since 1991 several probabilistic studies of seismic hazard (PSH) for Peru have been developed. These include those developed Sharma and Candia-Gallegos (1992) and Alva and Castillo (1993), which were used to update the Peruvian seismic code E.030

(SENCICO, 1997). Subsequently, the studies carried out by the Geophysical Institute of Peru (IGP, 2014) and that of Aguilar et al. (2017), which have a free access web application SENCICO (2017), for calculating the seismic hazard of the Peruvian territory. Both studies have served as the basis for updating the Peruvian code E.030 (2018).

The PSH developed for Peru, typically provide maps for peak horizontal ground acceleration of spectral response at 0.2, and 1.0 s periods with 10 % and 2 % probabilities of exceedance in 50 years, in hard soil (S1, according to code E.030). Only SENCICO's web application allows generating seismic hazard curves (SHC-Spectral Acceleration vs Annual Exceedance Probability), for structural periods of up to 3.0s. This has motivated the development of a PSH to obtain the SHC for 11 cities in the Peruvian territory with the largest population and economic movement. The SHC was constructed considering the requirements established in the Peruvian code E.030, for two types of soil and the zone with the highest intensity (Z4). The types of soil considered were intermediate soil (S2) and soft soil (S3), with mean shear wave velocities between 550-350, 350-180, respectively. For SHA, the seismic sources from the IGP (2014) and Aguilar et al. (2017) studies were used. For the seismic sources, 2 models were developed with a different combination of Ground Motion Prediction Equations (GMPE). The seismic sources defined in the two studies were grouped in the interface, intraplate, and continental subduction zones. For the interface and intraplate subduction sources, the GMPE of Young et al. (1997), Atkinson and Boore (2003), Zhao et al. (2006), BC-Hydro-Abrahamson et al. (2015), and Montalva et al. (2017), were used and for continental seismic sources, the GMPE of Sadigh et al. (1997) was used. Finally, a simple criterion through the average seismic hazard curve was used to represent the seismic hazard of the 11 selected cities. Figs. 1a to 1c and 1d show the seismic hazard curves for types of soil S2 and S3 and structural vibration period of 3.0 s and 3.5s, respectively. The GMEPs shown are the basis of the geometric mean of two orthogonal horizontal components of ground motion because that description is embedded in the GMEPs models.



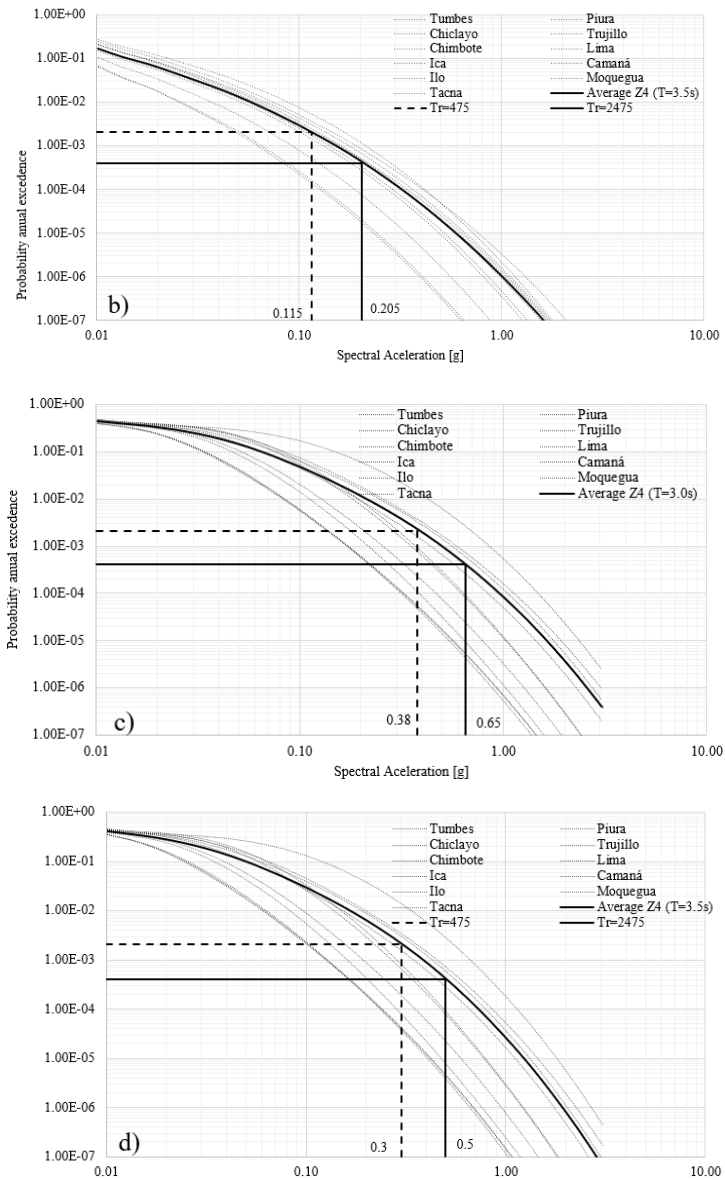


Figure 1 - Hazard curve period of 11 cities of Peruvian territory with the highest intensity for the structural vibration period (T) and soil types a) T= 3.0 s – S2 b) T= 3.5 s – S2 c) T= 3.0 s – S3 and d) T= 3.5 s – S3

Fig. 2 shows the coefficient of variation for soil types S2, S3, and the structural vibration period of 3.0 s and 3.5 s. It is clearly shown that there is a higher CV for the seismic danger curves in soil type S3, with maximum values of 1.06, 1.17, 1.89, and 1.93 for soils S2 and S3 and structural periods T= 3.0 s and T= 3.5 s, respectively.

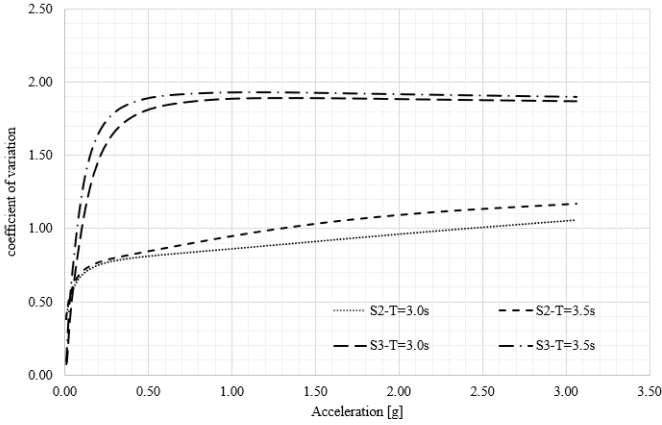


Figure 2 - Coefficient of variation for soil types S2, S3 and structural vibration period of 3.0 s and 3.5 s

4 Directional Effects

4.1 Database of the Peruvian seismic records

A set of 197 pairs of seismic accelerations records measured in Peru from 40 earthquakes events was selected. Each one has two horizontal components of ground motion (EW and NS components), with a focal depth of less than 40 Km and moment magnitude (M_w), surface-wave magnitude (M_s), and body-wave magnitude (M_b) more than 6. The records can be accessed through the Peruvian database of the network accelerographic belong to CISMID FIC/UNI – REDACIS and the database of the Geological Institute of Peru.

The records were grouped into three types of soil according to the calculation of the mean period (Eqn. 1), that is the best-simplified frequency content characterization parameter according to (Rathje et al., 1998), and the range of Table 6 taken from the Peruvian code for BIS (SENCICO, 2019). Through this procedure a total of 71 records were classified as soil type S1 (hard soil), with T_m less than 0.30 s, 42 records were classified as soil type S2 (intermediate soil), with T_m less than 0.40 s, and 84 records were classified as soil type S3 (soft soil), with T_m less than 0.60 s.

The upper cut off period for the response spectral acceleration was 4 s.

$$T_m = \frac{\sum_i \frac{C_i^2}{f_i}}{\sum_i C_i} \quad (1)$$

Where C_i represents the Fourier amplitude coefficients and f_i the discrete fast Fourier transform (FFT) frequencies between 0.25 and 20 Hz with frequency intervals Δf used in FFT computation, not greater than 0.05 Hz

4.2 Ratio maximum direction ground motions (MD) to geometric mean uniform-hazard spectral accelerations

As mentioned above the GMPEs are derived based on the geometric mean (S_{gm}) of two orthogonal horizontal components of ground motion combined as Eq. 2.

$$S_{gm} = \sqrt{S_x \cdot S_y} \quad (2)$$

Where, S_x and S_y are de the acceleration response spectrum in direction East-West and North-South direction, respectively and S_{gm} is the geometric mean.

The S_{gm} is traditionally been preferred because somewhat reduces the data dispersion, represented by logarithmic standard deviation term, (Baker and Cornell, 2006; Watson-

Lamprey, Jennie and Boore, 2007), as well as is a good estimate of the central value of randomly oriented individual components, the variability of which can be dealt with through modification of the standard deviation term. However, as noted by Boore et al. (2006), the S_{gm} depends on the orientation in which the components were measured or to which they were subsequently rotated. Consequently, the probability that the pseudo-spectral acceleration along a random orientation exceeds the geometric mean or the quadratic mean is high, 50% according to Beyer and Bommer (2008) and Hong and Goda (2007). Another definition that retains the two horizontal components, is Maximum-Direction spectral acceleration (MD), which is systematically higher than those for the geometric mean by factors ranging from 1.2 to 1.5 depending on the oscillator period. The MD or major-axis spectrum is determined by calculating the maximum response spectrum of a single-degree-of-freedom (SDOF) based on both horizontal components and is identified by the point on the orbit that gives the highest value of spectral response farthest from the origin, for a certain structural vibration period and angle θ (Hong and Goda, 2007; Huang et al., 2010; Huang et al., 2008; Judd and Charney, 2014; Stewart et al., 2011).

The trace of response spectrum orbit of a single lumped mass oscillator with direction-independent stiffness to bidirectional ground motion and the identification of the MD are shown in Fig.3. The two axes (X and Y) refer to the directions in the horizontal plane in which ground motion is recorded. Figs. 3a to 3c shows the spectral response (RS) of accelerations (S_a), velocities (S_v), and displacements (D), respectively, of SDOF systems with structural vibration period $T = 2.5$ s. The earthquake acceleration time histories are of the earthquake event of May 26, 2019, with a moment magnitude $M_w = 7.5$ and a depth of 141 km, register by the UNC D291 station. Figs. 3a to 3c show the RS in three-dimensional form, built over time values on the longitudinal axis (t) and the RS in X and Y for the other two axes. Also, the projection of the RS in the planes t-X, t-Y and X-Y are showed. Figs. 4a to 4c shows the orbit curves generated by the RS projection of acceleration, velocities, and displacements, respectively, on plane X-Y, as well as, the line that defines the MD corresponds to the maximum value of the combination of the square root of the sum of the squares of the spectral response X and Y (Eq.3). Moreover, the value of MD for accelerations, velocities, and displacements is different, besides, occurring at different time instants.

For this example, the maximum RS of accelerations is 33.07 cm/s^2 for a time instant of 16.85 s. For this instant of time, the maximum RS of velocities is 4.981 cm/s and displacements of 5.18 cm. These values are different from the MD of velocities of 15.031 cm/s for a time instant of 162.33 s and of displacements of 5.21 cm for a time instant of 162.89 s. The difference is notable for the spectral response in velocities (greater than 300%) and less significant in displacements (0.50%). Therefore, considering the maximum spectral response of accelerations for the design of systems that depend fundamentally on speeds can be detrimental. It is also important to note that the definition of MD adopted in this article is not related to the main axes of a structure, as it is confused in common practice in Peru.

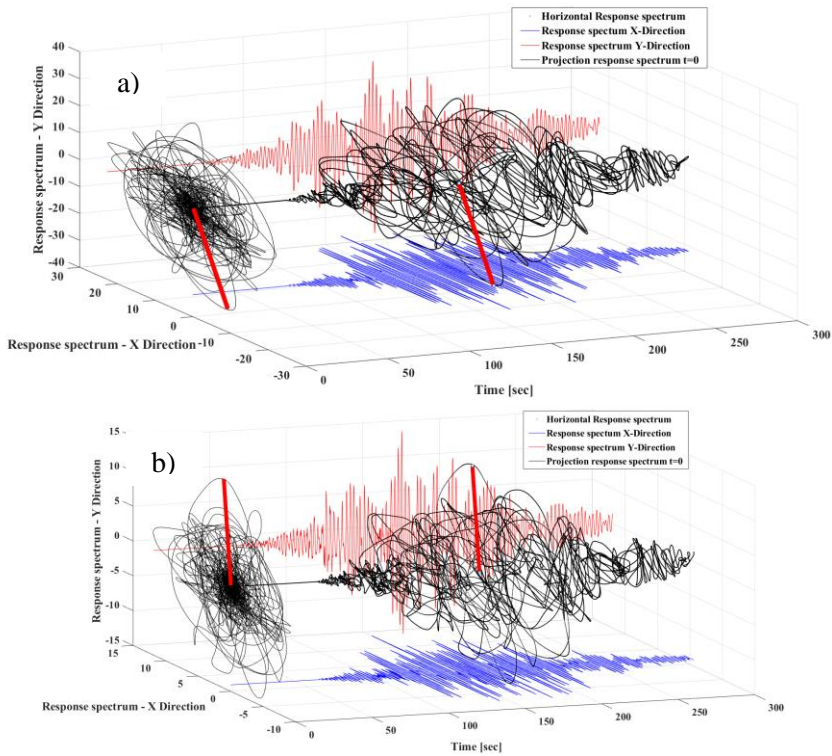
The definition of MD is particularly important for some structural systems such as the BIS because do not have preferred directions of response and have equivalent dynamic properties in all horizontal directions, having azimuth-independent properties. For BIS with azimuth-independent properties, the single lumped mass oscillator model that is the basis for MD ground motions is a good analog to the real system.

BIS has structural configurations for which the MD is the best indication of bidirectional demand, because, will usually have a similar period in each direction, and is designed to remove torsion from the overall dynamic response. The response quantity

of interest in the design of BIS is the peak resultant displacement, which is independent of the orientation angle of the input ground motion and can be characterized by the major-axis spectrum (Damian, 2011; Stewart et al., 2011).

The algorithm for calculating the MD response ordinate for a given period does not require considering a range of possible values for θ and taking the maximum overall calculated values. The response of a SDOF oscillator to a rotated ground-motion record can be expressed as a function of rotation angle and time and can be calculated differentiated concerning orientation angle, and then evaluated for the maximum value in time (Eqs. (3) and (4)). Grant (2004) used these equations to determine the major-axis spectra for a suite of records for the analysis of simple seismically isolated bridge models. Other researchers such as Hachem (2004), used the definition of MD to calculate the bidirectional response spectrum in the BIESPEC software.

Huang (2008) used the MD to calculate scale factors that transform rotated geometric mean of horizontal spectral demand, termed NGA-predicted GMRotI50 to a maximum spectral demand MD in the near-fault region in the western and central and eastern United States (Grant, 2004; Hachem, 2004; Huang et al., 2008).



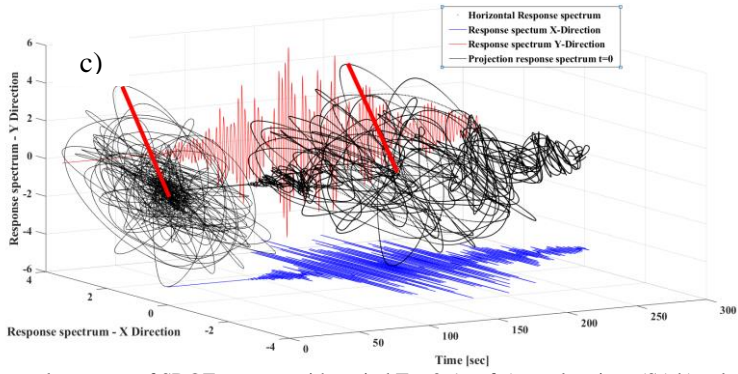


Figure 3 - Spectral response of SDOF systems with period $T = 2.5$ s of a) accelerations (S_a) b) velocities (S_v), and c) displacements (D),

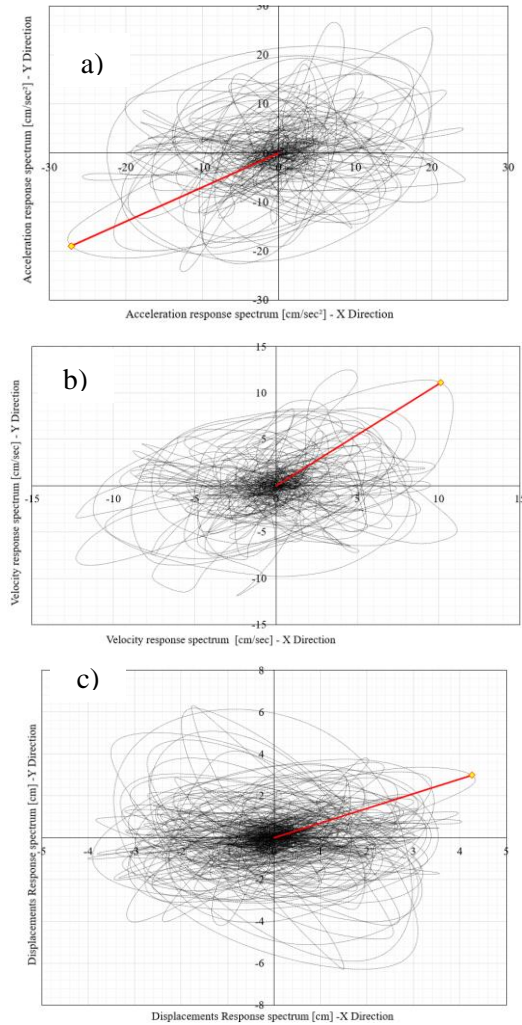


Figure 4 - Orbit curves generated by the RS projection on plane X-Y of a) acceleration, b) velocities, and c) displacements.

$$MD_{T_j} = \left(\sqrt{RS_{x,ti,T_j}^2 + RS_{y,ti,T_j}^2} \right)_{max} \quad (3)$$

$$\theta = \tan^{-1} \left(\frac{RS_{x,ti,T_j}}{RS_{y,ti,T_j}} \right) \quad (4)$$

Where RS_{x,ti,T_j} and RS_{y,ti,T_j} are the response spectrum for the original orientation angle by the time t_i a structural vibration period (T_j) for horizontal component East-West and North-South. MD_{T_j} is de the maximum response spectrum for structural vibration period T_j and θ is the exact peak response angle that can be calculated immediately from the vector sum of the two-time series.

There are several definitions of spectral ordinates expressed as a single value derived from the vector of the two perpendicular horizontal components such as the summary by Beyer and Bommer (2006). The most common of these is the principal direction (PD), the envelope spectrum ($RS_{envelope}$), the square root of the sum of squares spectrum (RS_{SRSS}), and the definitions GMRotD50 and GMRotI50 proposed by Boore et al. (2006).

The principal directions are determined considering that the seismic ground motion is a random process for which the principal axes can be determined as the set of axes for which the covariance disappears. Consequently, the cross-correlation $\rho_{xy} = \mu_{xy} / (\sigma_x \sigma_y)$ is zero and the variances σ_x^2 of the two horizontal components maximum and minimum, respectively, can be calculated from the analogy of Mohr's circle, with the Eqs. (5) to (8). Furthermore the angle θ_p between the x-axis, and the major principal axis can be written in terms of the variances σ_x and σ_y and the covariance μ_{xy} of the two horizontal components of the seismic ground motion $a_x(t)$ and $a_y(t)$ through the Eq. (8) (Clough and Penzien, 1993; Fernandez-Davila, 2007).

$$\sigma_x^2 = \frac{1}{t_d} \cdot \int_0^{t_d} (RS_x(t) - \overline{RS_x(t)})^2 \cdot dt \quad (5)$$

$$\sigma_y^2 = \frac{1}{t_d} \cdot \int_0^{t_d} (RS_y(t) - \overline{RS_y(t)})^2 \cdot dt \quad (6)$$

$$\mu_{xy}^2 = \frac{1}{t_d} \cdot \int_0^{t_d} (RS_x(t) - \overline{RS_x(t)}) \cdot (RS_y(t) - \overline{RS_y(t)}) \cdot dt \quad (7)$$

$$\theta_p = \frac{1}{2} \cdot \tan^{-1} \left(\frac{2 \cdot \mu_{xy}}{\sigma_x^2 - \sigma_y^2} \right) \quad (8)$$

Where, σ_x , σ_y are the variances of the two horizontal components of the seismic ground motion $RS_x(t)$ and $RS_y(t)$, respectively, and μ_{xy} their covariance.

The envelope response spectrum RS_{env} is another definition derived from the vector of the two orthogonal horizontal components, which is defined as the larger spectral ordinate of the x and y components at each structural vibration period and is computed with the Eq. (9).

$$RS_{env} = \max(RS_x, RS_y) \quad (9)$$

The square root of the sum of the square spectrums RS_{SRSS} is used in several codes to combine the individual spectrum of each component x and y, and is computed with the Eq. (10).

$$RS_{SRSS} = \sqrt{RS_x^2 + RS_y^2} \quad (10)$$

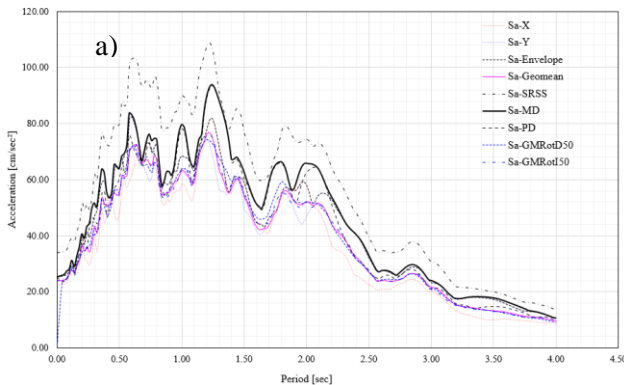
Finally as noted by Boore et al. (2006) the geometric mean of the response spectra of two orthogonal horizontal components of seismic ground motion depends on the

orientation in which both components were measured. For this reason, Boore et al. (2006) introduced two orientation-independent measures of mean spectral demand, which aim at reducing the variance of the ground-motion measure and at producing less arbitrary approximations to components that have genuinely random orientation, GMRotD50, and GMRotI50 (Beyer and Bommer, 2007; Damian, 2011). The former by GMRotD50 is defined by calculating the geometric mean spectral response for all possible orientations of the original ground-motion (0° to 90°) and taking the median value over all the angles. The orientation corresponding to the median value is independent of the original orientation of the horizontal components but results in a response spectrum for which every period is controlled by a different orientation angle (Beyer and Bommer, 2006; Damian, 2011). The other spectral response definition introduced by Boore et al. (2006) GMRotI50, is an approximation of GMRotD50 with a constant axis orientation for all periods, which minimizes the sum of differences between GMRotD50 and GMRotI50 overall considered periods. GMRotI50, provides a measure for which each spectral ordinate is derived from a common orientation angle. The writers recommend that it is important “to choose the structural vibration period range (T_h) large enough so that all peaks in the displacement response spectrum are included and to have enough values of the oscillator period to define each peak in the response spectrum” (Boore et al. 2006). However, how as noted by Damian (2011) although this may be applicable when providing a single measure of response that can be used for a range of structural periods, it would seem important to consider for some cases of particular structures. As previously mentioned, the PSH carried out in Peru that is used for the calculation of seismic demand has been estimated based on the geometric mean (geomean) of two horizontal components.

The GMPE in Peru has been developed based on a geomean combination of ground motion. Therefore, in this paper to consider the effect of the direction of horizontal seismic demand, the directional ratio (DR) between the spectral response directional combination of two horizontal components ($RSDC$), and the response spectrum geometric mean ($RS_{geomean}$) has been calculated (Eq. 11).

$$DR = \frac{RSDC}{RS_{geomean}} \tag{11}$$

An example of direction combination of the response spectrum by accelerations (S_a), velocities (S_v), and displacements (D), is shown in Figs. 5a to 5c respectively, for earthquake events of 2019 Alto Mayo. Note that there is a marked difference between the D-MD and the D-Geomean value long period zone.



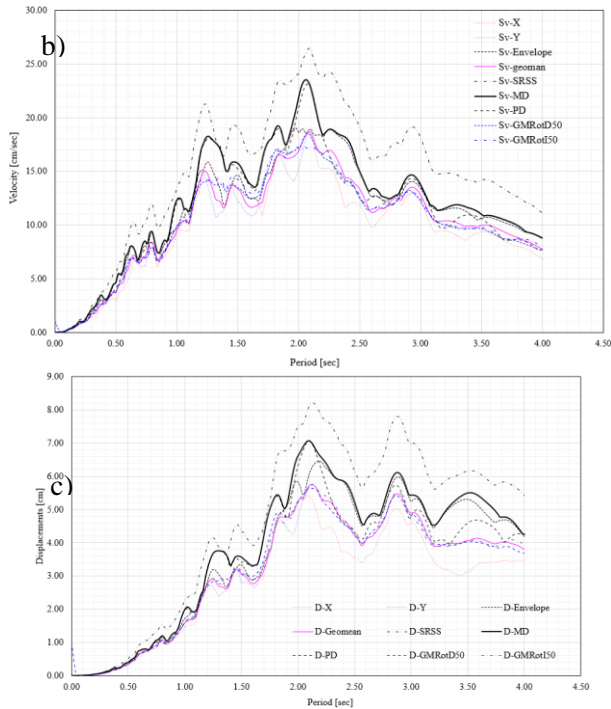


Figure 5 - Response Spectral a) using different definitions for earthquake events of 2019 Alto Mayo for a) accelerations (S_a), b) velocities (S_v) and c) displacements (D),

In this paper, to consider the effect of the directional combination of horizontal seismic demand, the DR was calculated from a set of 197 earthquake acceleration time histories from 40 earthquake events of Peruvian database, grouped into three types of soil: hard soil (S1), intermediate soil (S2), and soft soil (S3).

Fig. 6 shown the ratio $RSDC/RS_{Geomean}$ average for soil types S1, S2, and S3. The ratios of GMRoTi50 and GMRotD50 are similar to Geomean and vary at most up to 6%. MD ratios are higher than DP with maximum values of 1.32 compared to 1.21 DP. The SRSS ratios reach values of 1.49, which are the maximum values obtained, however, this combination is excessive since it is considered the result of the maximum spectral ordinates that occur at different instants of time. Fig. 7 shows the influence of soil type on the directionality factors obtained with the combination of MD, for displacements (7a), velocities (7b), and accelerations (7c). It can be seen that the soil influences directionality factors for high periods, reaching maximum values of 1.35. The most affected response is that of displacement, followed by that of acceleration and finally of velocities. Fig. 8 shows the coefficient of variation (CV) of the MD / Geomean directionality factor for soil types S1, S2, and S3 considered. It is appreciated that the CVs are smaller for the velocity response and are similar for the displacement and acceleration response. Also, it is appreciated that the highest values of CVs occur for areas with periods of less than 1.5s.

Finally, Fig. 9 compares the MD/Geomean directionality factors obtained with the Peruvian records with those proposed by other researchers for the United States area. It can be seen that the values obtained are similar to those obtained by Huang et al. (2010) for the Western US Far-Field and near Field. The NEHRP that were adopted by the ASCE SEI 7-5/10 and 16 and other values are higher.

Based on the results obtained, it could reasonably use a factor of 1.30 (average value for periods greater than 2.0 s) to amplify the geometric mean values to obtain the maximum direction values.

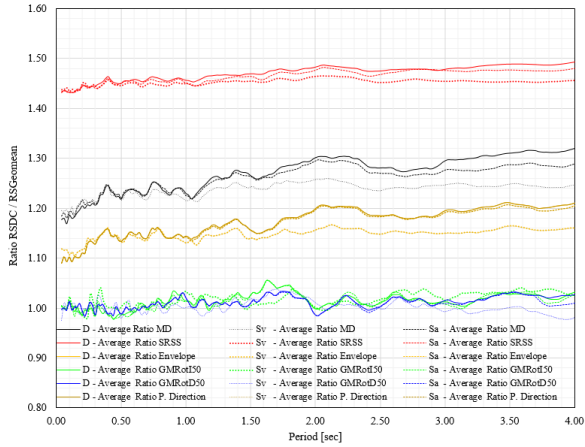
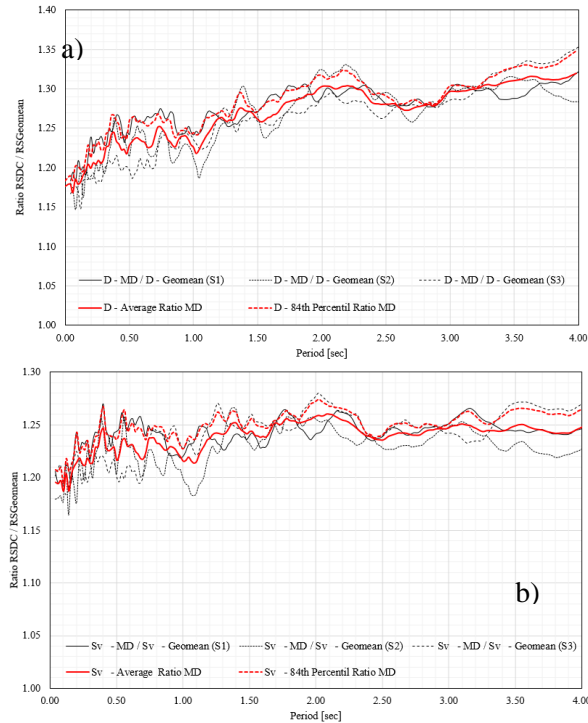


Figure 6 - Ratio RSDC/RSGeomean average for soils types S1, S2, and S3.



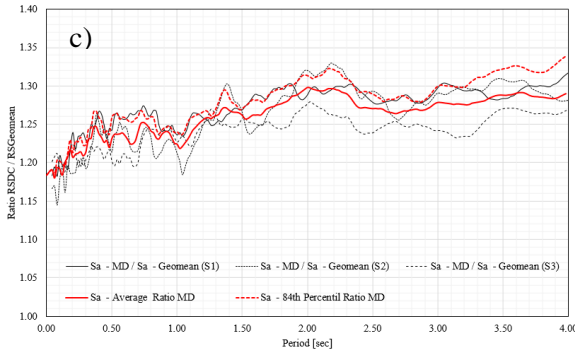


Figure 7 - Influence of soil type on the directionality factors obtained with the combination of MD, for a) displacements, b) velocities, and c) accelerations.

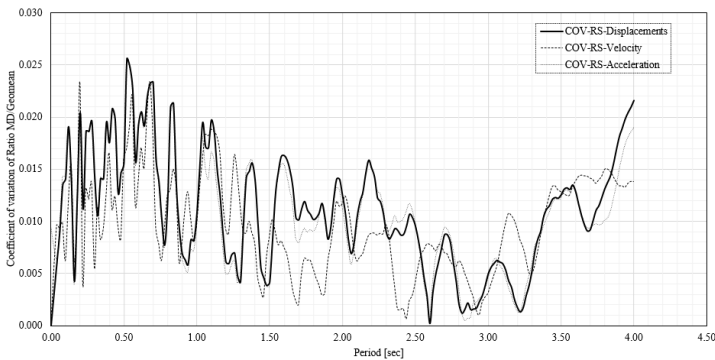


Figure 8 - Coefficient of variation (CV) of the MD/Geomean directionality factor for soils types S1, S2 and S3

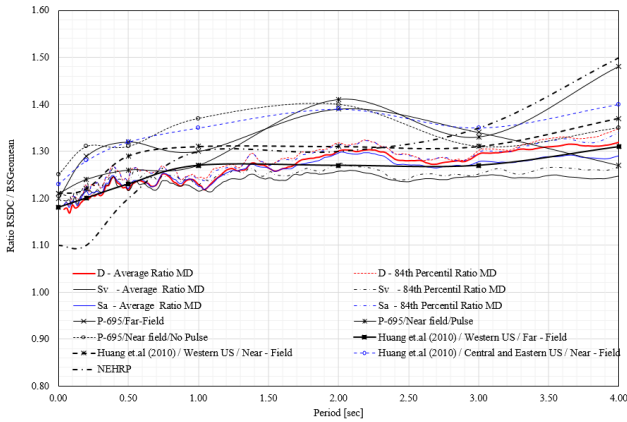


Figure 9 - Comparison of the MD/ Geomean directionality factors obtained with the Peruvian records with those proposed by other researchers for the United States area

5 Fragility Function

Fragility is an inherently uncertain quantity subject to multiple sources of both aleatory (randomness) and epistemic (lack of knowledge) uncertainty (Ellingwood and Kinali, 2009; Kiureghian and Ditlevsen, 2009). Typically, record-to-record variability in the intensity measures (IMs) and engineering demand parameters (EDPs) relationship is treated as aleatory, due to the natural randomness of ground motions. This source of variability is quantified directly by Nonlinear Response Time History Analysis

(NRTHA), using a sufficiently large number of ground motions. Epistemic uncertainty comes from lack of knowledge (ignorance) and includes: model-type uncertainty, referring to imperfect modeling capabilities, especially considering that simplified models are typically used for computational efficiency reasons and method-related uncertainty, due to imperfect methodology (e.g., a bad regression; an insufficient IM; or a deficient analysis approach). Sources uncertain that may be either one or (usually) both, leaning toward aleatory when a new structure is concerned, versus a combination of both when an existing structure is assessed are the model-parameter uncertainty due to incomplete knowledge or actual randomness in the model properties (e.g., strength, ductility, mass, or stiffness) and limit state capacity uncertainty, due to unknown or random EDP thresholds resulting from experiments or expert judgment (Bakalis and Vamvatsikos, 2018). The effects of modeling uncertainties must be combined with the effects of record-to-record variability and this can be done following different approaches. In this study, it assumes that modeling uncertainty is also lognormally distributed and that random variables associated with epistemic and aleatory uncertainty are independent. These uncertainties were propagated in the fragility analysis by using Latin Hypercube Sampling (LHS). LHS is a stratified-random procedure that provides an efficient way of sampling random variables from their distributions and ensures that the set of samples reflect the entire range of all the parameters (McKay et al., 1979).

The aleatory uncertainty of the parameters affecting the seismic response was reflected using a suite of 30 earthquake ground motion records. The model-parameter uncertainty was considered by using a total of 4 modeling parameters presented in Table 1, with their average and standard deviation that defined the lognormal distribution CDF. In this study, it assumes that the logarithmic standard deviation (β) for the stiffness of the rubber bearing (K_{RB}) of 0.50. This value reflected the performance variation of the rate of change of causes of how manufacturing variation, aging, temperature change which affect shear properties, for Bridgestone Seismic Isolation Product, taken as a reference for the case study.

The equivalent shear stiffness (K) and equivalent damping ratio (ξ) are dependent on each other. For the high damping rubber bearing the indicated rate of change of equivalent damping ratio (ξ_{RB}) are corresponding to both maximum and the minimum rate of change of shear stiffness (K_{RB}) and are adopted how 0.30. For stiffness of the superstructure (K_{SE}), it adopted 0.27 for logarithmic standard deviation (β). Also, the variability in damping is not the same as variability in response due to damping. Therefore, β for the equivalent damping ratio of the superstructure (ξ_{SE}) was calculated from the response for median damping R_m and response for $R_{.1\beta}$ damping using Eq. (12). For reinforced concrete structures (considerable cracking), $R_m = 5\%$ and $R_{.1\beta} = 3\%$, $\beta = 0.51$, (EPRI, 2010; Kennedy, 2015).

Finally, Fig. 10 shows the model-parameter uncertainty of a total of 4 modeling parameters presented in the suite of 30 analysis (one for each earthquake ground motion records).

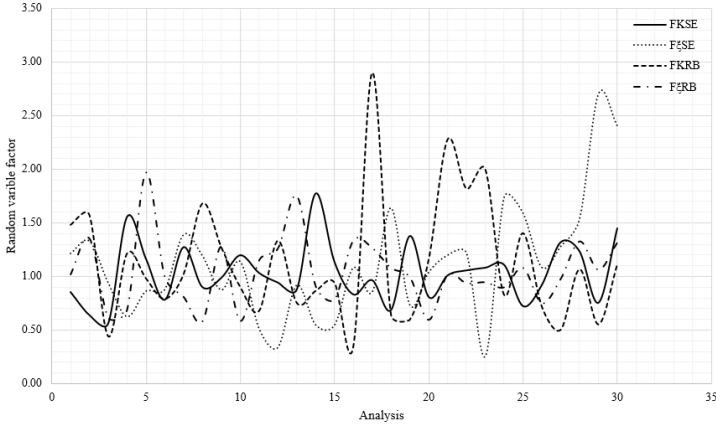


Figure 10 - Factor for Random variable

Table 1 - Statistical distributions of the uncertain modeling parameters

CDF parameters	Rubber isolators		Superstructure	
	Stiffness K_{RB}	Damping ξ_{RB}	Stiffness K_{SE}	Damping ξ_{SE}
Median (θ)	1.0	1.0	1.0	1.0
Logarithmic standard deviation (β)	0.50	0.30	0.27	0.51

5.1 Seismic ground motion

30 scaled records for soil type S2 and S3 were selected according to the ASCE/SEI 7-16 (2016) standard to match the design spectrum of the Peruvian technical standard for seismically isolated structures SENCICO E.031 (2019), to accurately characterize either the mean response or the effect of the seismic acceleration record on the variability in response. Each pair of horizontal components of the 30 seismic ground motions was scaled such that the average value of the maximum direction (MD) does not fall below the target spectrum (TS) in a structural vibration period range of 1.5 s to 4.0 s. In this study, the MD is the 5% damped spectral response ordinates calculated with Eq. 3 and the TS is the elastic design spectrum of the E.031 (2019) code, defined with Eqs. 12 to 16 and the parameters of Table 2. In this study, the design spectrum of the code E.031 was amplified by a directional ratio (DR) estimated at 1.30.

The structural vibration period range of $0.75 \cdot T_1$ to $1.25 \cdot T_1$ (approximately equal to 1.5 s – 4.0 s) is useful for scaling of the acceleration seismic records of the ground motion to accurately represent the Peruvian seismic hazard, according to the code E.031 (SENCICO, 2019). In this case, T_1 is the fundamental structural vibration period of the BIS, typically greater than 2.0 s.

$$S_a = 1.5 \cdot Z \cdot C \cdot S \cdot g \quad (12)$$

$$T < 0.2 \cdot T_P \quad C = 1 + 7.5 \cdot \frac{T}{T_P} \quad (13)$$

$$0.2 \cdot T_P \leq T < T_P \quad C = 2.5 \quad (14)$$

$$T_P \leq T < T_L \quad C = 2.5 \cdot \frac{T_P}{T} \quad (15)$$

$$T_L \leq T \quad C = 2.5 \cdot \frac{T_P \cdot T_L}{T^2} \quad (16)$$

Where S_a is the pseudo-acceleration, C is the seismic amplification factor, Z is the zone factor (PGA), S is the soil amplification factor, T_P is the period defined by the factor C platform with constant velocity, T_L is the period that defines the start of the zone of factor C with constant displacement, T is the structural period.

Table 2 - Soil-type dependent parameters required to construct the Peruvian target design spectrum (TS) for damping ratio equal to 5% (SENCICO, 2019)

Parameter	Soil type		
	S1	S2	S3
S	1.0	1.05	1.10
T_P (s)	0.4	0.6	1.0
T_L (s)	2.5	2.0	1.6

The acceleration records were selected using the procedure of amplitude scaling. This procedure was used because it has some advantages resulting from the fact that only the amplitude is modified and the records maintained all individual characteristics, except the amplitude (Mazzoni et al., 2012; Fernandez-Davila and Mendo, 2020; Reyes et al., 2014).

The procedure to match the response spectral to the TS was as follows:

1. Calculation of the elastic acceleration response spectral for damping ratio of 5% of each pair of horizontal components (EW and NS) in a range of periods of 0.0 s to 4.0 s with a step of 0.02 s.
2. Calculate the SRSS of the 5% damped spectral ordinates from ground motion pairs.
3. Scaled each ground–motion pair by a first factor (FPGA), calculate how the ratio between PGA of the TS and the SRSS combination of each ground–motion pair.
4. Calculate the average of SRSS of a ground–motion pair of all possible combinations of 11 acceleration records, which is the number of records indicated in the procedure of ground motion selection in the ASCE/SEI 7-16 (2016) code.
5. Calculate the root-mean-square error (RMSE) between SRSS of each combination and TS using Eq. 17. For this processing, a MATLAB's script was developed using the `nchoose(n, k)` command, in which n is the number of possible choices and k is the number of records:

$$RMSE = \sqrt{\frac{1}{n} \cdot \sum [\ln(Ps a_{SRSS,i}) - \ln(Ps a_{TS,i})]} \quad (17)$$

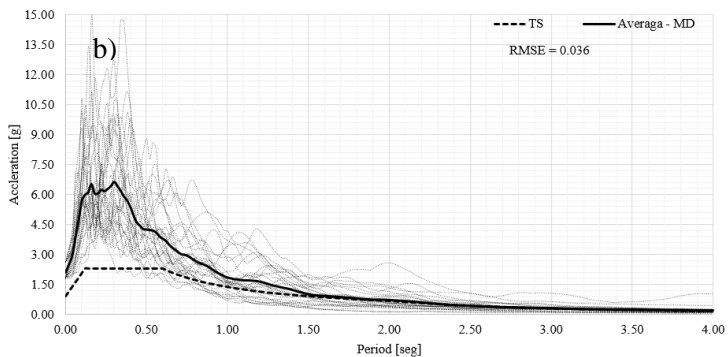
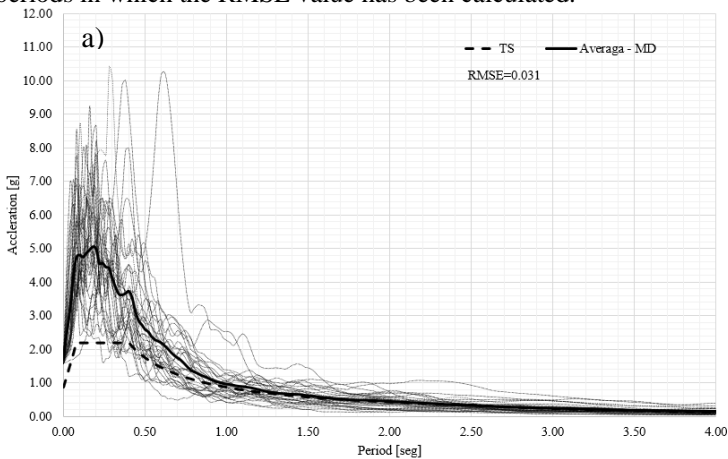
where \ln is the natural logarithm, n is the number of data, and MSE is the mean squared error, $Ps a_{SRSS,i}$ is the ordinate of the SRSS and $Ps a_{TS,i}$ is the ordinate of the TS.

6. Tabulate the 30 acceleration records with the lower RMSE values for each soil type.
7. Finally, apply a second factor such that the RMSE between TS and the average of the 30 pairs scaled records combined how the SRSS of each ground–motion pair ($SRSS_{average}$), is the minimum, in a range of periods from 1.5 s to 4.0 s.

Table 3 shows the information on the accelerographic stations and the parameters of the 30 records selected for the soil types S1, S2, and S3, and Figs. 11a and 11b show the scaled records to do the match between the average of the MD response spectrum and the TS in a range of periods of 1.5 s – 4.0 s.

The selection of the 30 records with the lowest RMSE value between the TS and the average of the MD response spectrum combination of each pair of horizontal records generates an excellent approximation in the range of periods of interest. The RMSE values calculated in a previous study conducted by (Mendo and Fernandez-Davila, 2020) were 0.021, 0.022, and 0.031 for the soil's types S1, S2, and S3, respectively. Unlike this study, in the previous study, the selection and adjustment of the records were carried out with 11 records such as the square root of the sum of the squares (SRSS) of the 5% damped spectral ordinates that matched to the TS (elastic design spectrum of the E.031 (2019) code).

The study conducted by Saez et al. (2012) in Chile shows higher RMSE values than those calculated in this study. They used the scaling procedure described by Kottke and Rathje (2008) to select the records. The RMSE calculated by Saez et al. (2012) in an approximate range of 0.2 s – 3 s, for all possible combinations of seven acceleration records for three soil types, concerning the elastic design spectrum of the Chilean NCh2745 (2003), was 0.21, 0.25, and 0.31 for soil types such as S1 (hard soil), S2 (intermediate soil), and S3 (soft soil), respectively. The RMSE values obtained in both studies were much lower than the minimum value calculated in the study of Saez et al. (2012) of 0.21. Although the reason for the difference is not clear, this may be due to the range of periods in which the RMSE value has been calculated.



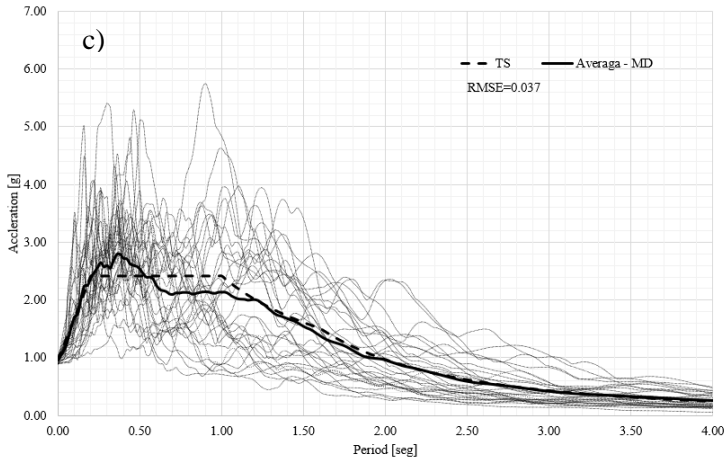


Figure 11 - Match between TS and the average response spectra of the 11 scaled records in the range of the periods of 1.5 s – 4.0 s for soil types: (a) S1, (b) S2, and (c) S3.

Table 3 - Earthquakes considered in the database

Earthquake	Date	Magnitude	Epicenter		Depth [km]	Number of records			
			Latitude [°S]	Longitude [°W]		S1	S2	S3	S-T*
Lima	17-10-1966	Mw=8,1	10.70	78.70	24.0	1	0	0	1
Ancash	31-05-1970	Ms=7.8	9.36	78.87	64.0	1	0	0	1
Lima	05-01-1974	Mw=6.5	12.39	76.29	91.0	0	0	1	1
Lima	03-10-1974	Ms=7.8	12.50	77.98	13.0	1	0	0	1
Arequipa	23-06-2001	Mb=6.9	16.08	73.77	33.0	0	1	0	1
Arequipa	07-07-2001	Mb=6.5	17.4	71.67	33.0	1	0	0	1
Ica	13-06-2005	Mw=7.8	13,67	76,76	146.0	2	0	2	4
Tarapaca	13-06-2005	ML=7.2	19.61	69.97	146.0	2	2	0	4
Loreto	25-09-2005	ML=7.0	5.80	76.20	115.0	0	0	1	1
Ica	15-08-2007	Mw=8.0	13.67	76.76	40.0	2	0	2	4
Tacna	05-05-2010	ML=6.5	18.34	71.17	36.0	1	1	0	2
Anchash	24-08-2011	ML=7.0	9.50	76.00	149.0	4	1	0	5
Ica	28-10-2011	Mw=6.9	14.44	75.97	24.0	0	1	1	2
Tacna	14-05-2012	ML=6.1	18.05	70.06	98.0	1	0	0	1
Arequipa	07-06-2012	ML=6.1	15.98	72.75	110.0	1	0	0	1
Ica	30-06-2012	ML=6.3	14.37	76.02	54.0	5	2	0	7
Ucayali	02-08-2012	ML=6.4	8.64	74.19	150.0	3	0	0	3
Ucayali	10-11-2012	ML=6.0	8.89	75.12	146.0	3	0	0	3
Arequipa	25-09-2013	ML=9.0	16.26	74.98	37.0	3	1	0	4
Tarapaca	04-01-2014	Mw=8.2	19.57	70.98	38.90	0	0	2	2
Arequipa sea	15-03-2014	ML=6.2	14.34	76.58	16.0	2	2	0	4
Iquique	16-03-2014	Mw=6.7	19.96	70.81	20.6	0	0	1	1
Chile	11-02-2015	ML=6.7	23.12	66.59	190.0	2	0	0	2
Arica	22-03-2015	ML=6.2	18.76	69.75	125.0	4	0	0	4
Tumbes	05-06-2017	M6.2	4.17	80.66	18.0	1	1	0	2
Tarapaca	13-06-2017	ML=7.2	19.61	69.97	146.0	2	2	0	4
Arequipa	17-07-2017	Mw=6.3	15.61	73.46	100.0	1	0	0	1
Junin	13-08-2017	M6.1	10.76	74.77	15.0	1	0	0	1
Arica	10-10-2017	M6.3	18.91	69.86	100.0	0	1	0	1
Arequipa	14-01-2018	M6.9	16.07	74.89	48.0	3	4	8	15
Tarapaca	02-04-2018	M6.6	18.18	69.43	580.6	0	0	1	1
Ucayali	24-08-2018	M6.8	10.89	70.66	616	1	2	11	14

Table 3. Continued.

Earthquake Event	Date	Magnitude	Epicenter		Depth [km]	Number of records			
			Latitude	Longitude		S1	S2	S3	S-T*
Canar	06-09-2018	M6.4	2.17	78.82	80.0	1	4	0	5
Tarapaca	01-11-2018	M6.3	19.91	69.86	99.0	3	3	0	6
State of Acre	05-01-2019	M7.2	8.07	71.43	598.0	2	1	16	19
Loreto	08-01-2019	M6.3	4.41	73.82	15.0	0	0	1	1
Ica	24-01-2019	M6.0	14.79	75.75	50.0	7	6	0	13
Pastaza	22-02-2019	M7.7	2.00	77.19	113.0	5	2	20	27
Puno	01-03-2019	M7.0	14.84	70.22	270.0	4	1	14	19
Bolivia	15-04-2019	M6.3.	16.63	65.00	350.0	4	5	0	9
TOTAL						74	43	81	198

(*) S-T: Sub total

5.2 Case Study with Peruvian Draft Code E.031

The case of study is the four stories reinforced concrete hospital building that consists of moment-resisting frames and a symmetrical rectangular plan of 30 m wide and 70 m long (aspect ratio equal to 2.33). Story heights are assumed 4.5 m for all stories. The hospital is located in seismic zone 4 with soil condition defined as soil type S2 according to the E030 code (SENCICO, 2018).

The structural characteristics of the buildings (geometric dimensions, reinforcement ratios, structural details, etc.), have been derived according to the technical standards and design rules in force in Peru, (SENCICO, 2009, 2019). As far as the strength of materials is concerned, average compression strength (f'_c) of 28 MPa and yield strength (f_y) of 420 MPa have been assumed for concrete and steel, respectively. The floor height is 0.25m, the column sections are 0.70m x 0.70m, and the beam sections area is 0.40m x 0.90m. Fig. 12 shows a plan view of the building.

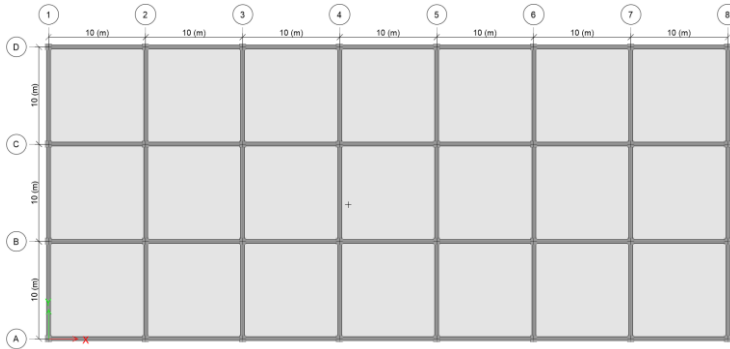


Figure 12 - Case study building, plan view

The design of isolation systems was carried out for MCE with the design spectrum defined in the E031 draft code (SENCICO, 2019) which is given by Eq. (18). For structural periods T greater than T_L , replacing the Eqs. (18) in (12), the following equations can be obtained:

$$PS_a = 1.5 \cdot Z \cdot 2.5 \cdot \left(\frac{T_p \cdot T_L}{T^2} \right) \cdot S \cdot g \quad (18)$$

$$S_d = \frac{PS_a}{\omega_n^2} \quad (19)$$

$$S_d = \frac{3.75 \cdot Z \cdot S \cdot T_p \cdot T_L}{4\pi^2} \cdot g \quad (20)$$

Where S_d is the maximum displacement design of response spectrum, Z is the zone factor (PGA), S is the soil amplification factor, T_p is the period defined by the factor C platform with constant velocity, T_L is the period that defines the start of the zone of factor C with constant displacement, T is the structural vibration period and g is the acceleration of gravity (9.80665 m/s^2)

For an S3 soil in the zone of highest seismicity Z4, considering also the damping modification factor (B), it can define the displacement used for the design of the isolation systems D in mm, by the Eq. 2.

$$D = \frac{528.17}{B} \quad (21)$$

The isolation systems considered are the high damping rubber bearings (HDRBs) from the series seismic isolation product line-up of Bridgestone (BRIDGESTONE, 2013). The HDRBs hysteretic model is assumed as bilinear with first stiffness K_1 and secondary stiffness K_2 , K_{eff} is the effective stiffness, Q is the characteristic strength, D is the maximum displacement, Q_y is the yield force at the yield displacement D_y , such as illustrated in Fig. 13. The ratio between primary stiffness to secondary stiffness (K_1/K_2) is assumed 10.0. The characteristics of designed LRB isolators are listed in Table 4.

The linear analysis which was carried out using an iterative process provided acceptable results of story drifts and floor acceleration, then nonlinear time history analysis was carried out using the information obtained from the linear analysis.

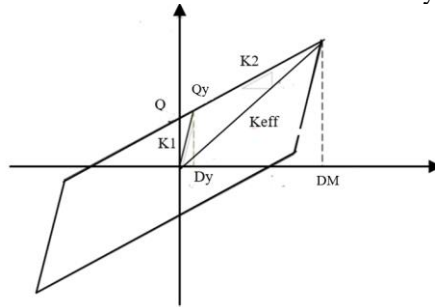


Figure 13 - The HDRBs hysteretic model assumed as bilinear

Table 4 - Nominal values of properties for the seismic isolators HDRB

Maximum displacements design	S_d	528.17	mm
Damping modification factors	B	1.35	
Displacements total maximum	$DM=1.5 \cdot S_d$	449.92	mm
Properties	HH150x4S		
Initial stiffness	K_1	13696.59	kN/m
Post yield stiffness	K_2	1369.66	kN/m
characteristic strength	Q	428.26	kN
yield force	Q_y	475.85	kN
yield displacement	D_y	34.70	mm
Equivalent stiffness	K_{eff}	2321.51	kN/m
Rubber height	H	200.00	mm
Fundamental period isolated-structures	T_i	2.93	s
Fundamental period for the building without seismic isolation	T_s	0.91	s

In the design two analysis was carried out. The first analysis was the response spectrum analysis (RSA) and the second was de the NRTHA that was carried using fast nonlinear analysis (FNA) (CSI, 2020). The NRTHA used seven pairs of records compatible with the maximum earthquake spectrum of E031 draft code (TS), such as spectral values of the SRSS average match a TS, such as shown in Fig. 14.

The records were selected using the procedure of amplitude scaling according to the procedure described above. The RMSE is 0.049.

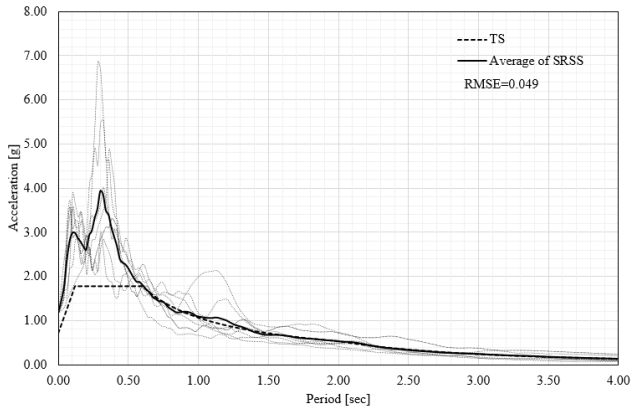


Figure 14 – Match between TS and the average response spectra of the 7 scaled records SRSS in the range of the structural periods of 1.5 s – 4.0 s for soil type S2.

Three models of the structure were analyzed according to the nominal, maximum, and minimum modification factors of properties (λ) for HDR. The first model considers the nominal values of properties for the seismic isolators (Table 3). The values of λ used for the second and third model were $\lambda \cdot K_d = 2$, $\lambda \cdot Q_d = 1.7$ and $\lambda \cdot K_d = 0.8$ and $\lambda \cdot Q_d = 0.8$. These minimum and maximum values for λ have been specified by the E.031 draft code (SENCICO, 2019).

In terms of drifts, the maximum λ is most critical as it increases the stiffness of the isolators and reduces the effectiveness by decreasing the structural period.

The drift ratios for the RSA and the nominal models from NRTHA are shown in Fig. 15 that is less than the established limits according to the draft code E.031 is 0.0035 for RS and 0.005 for NRTHA.

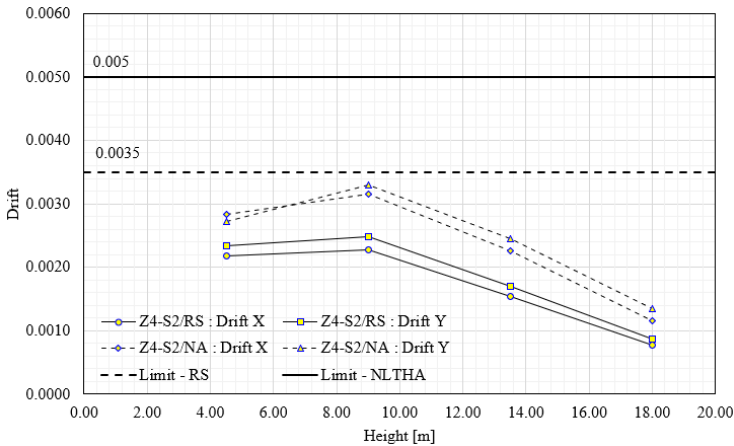


Figure 15 – Drift for RS and NRTHA and nominal model

5.3 Developing Collapse Fragility Functions

Collapse fragility functions have been derived through Incremental dynamic analysis (IDA) that has been preferred to better identify, for each ground motion pair, the earthquake intensity level at which collapse occurs.

IDA involves scaling each ground motion in a suite until it causes structure collapse (Vamvatsikos and Cornell 2002). This process produces a set of intensity measure (IM) values associated with the onset of collapse for each ground motion. The probability of collapse at a given IM level, z , can then be estimated as the fraction of records for which collapse occurs at a level lower than z . A plot of these probabilities is referred to as an empirical CDF. Fragility function parameters were estimated from this data by taking logarithms of each ground motion's IM value associated with the onset of collapse and computing their mean and standard deviation (Bakalis and Vamvatsikos, 2018; Vamvatsikos, 2014; Vamvatsikos and Cornell, 2004).

IDA has been carried out scaling a set of 30 ground motion pairs compatible (on average) with the TS associated with the highest available hazard data ($T_r = 2475$ years) and assuming the "effective" fundamental period of the isolated building at the collapse prevention limit state as conditioning period ($T^* = T(\text{PGA})$). The spectral acceleration at the fundamental period PGA ($S_a(\text{PGA})$) has been selected as an intensity measure. As said before, two sources of uncertainties have been considered: record-to-record variability and model variability. The record-to-record variability has been quantified directly through IDA. The mean estimates method has been then used to combine the effects of the two sources of variability, thus deriving the total dispersion of the fragility curve.

A simplified criterion for the superstructure collapse was adopted, based on thresholds average inter-story drift ratios of fragility medians generic building type C1M (Mid-Rise Concrete Moment Frame) and elastic period of 0.76 s according to the Hazus-MH 2.1 Technical and User's Manual (FEMA, 2001). The structural damage state thresholds extensive for seismic design level "moderate-code" is 0.0156. Figs. 16a to 16c shows the empirical CDF and the fitted log-normal fragility functions derived for this case of study for levels 1, and 2, which are those with the highest values of drift. The design earthquake intensity level (and the corresponding probability of collapse) prescribed by Peruvian E.031 Seismic Code and the acceleration of Average Hazard curve (Figure 1) amplified by a directional ratio (DR) estimated as 1.30, for structural vibration period $T = 3.0$ s and soil type S2 and $T_R = 2475$ years, are identifies

The ASCE 7-16 code establishes the acceptable probability collapse (APC) at maximum considered earthquake according to the risk category. APC of 2.5% is specified for Hospitals (category IV). On the CDF the APC OF 2.5% is marked. It can be seen that for all the cases analyzed the APC calculated is less than the limit of 2.5% established by the code ASCE/SEI4-16 (2016).

The failure modes of the isolation device depend on the type of isolation device used. For HDRBs, three failure modes can be considered, ie, cavitation, buckling, shear failure, and connections. As far as shear failure is concerned, only this type of failure was considered in this paper. Recent studies such as the Montuori et al. (2015) have pointed out a lower bound limit for rubber failure ranging between 260% and 380% in terms of shear deformation (γ), regardless of the shape factor of the bearing and the applied pressure. Such value seems to be rather conservative if compared with the experimental results reported by Muramatsu et al. (2004), where values of γ of the order of 400% to 500% have been found by Cardone et al. (2019). Prudentially, a limit shear strain of 250% has been assumed in this study. It is worth noting that this value also corresponds to the validity limit of the shear model by Grant et al. (2004), which governs the cyclic behavior of the selected HDR bearing element. The collapse of the isolation system is assumed to occur when shear strain in the isolation devices exceeds the limit of 250%.

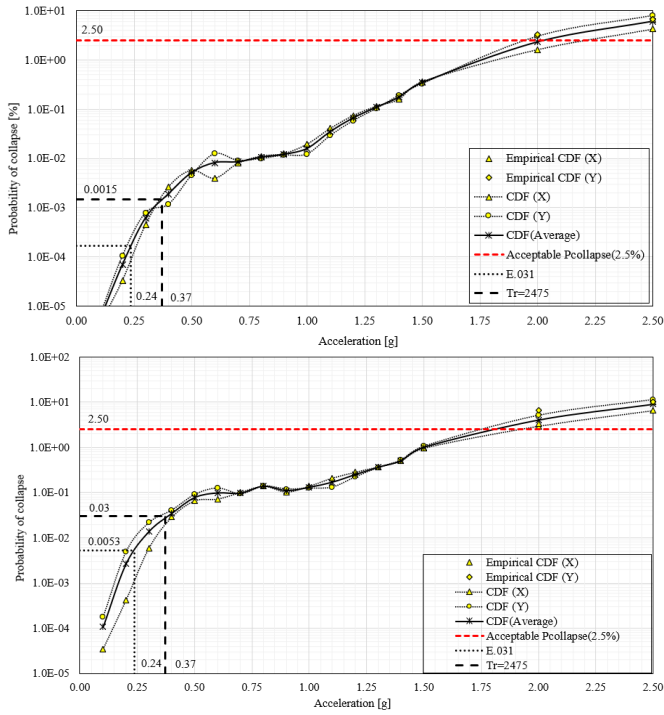


Figure 16 - Cumulative distributions and corresponding fitted collapse fragility functions for level a) One, b) Two

Fig. 17 shows the probability of collapse for the seismic isolation system and marks the APC of 2.5%. For the acceleration indicated by standard E.031 (0.24-g), as well as for the average acceleration of 11 cities, obtained in the seismic hazard study (Fig. 1a), amplified by the factor of 1.3 ($0.285 \cdot 1.30 = 0.37\text{-g}$), for the structural vibration period $T=3.0$ s, it is less than the limit. Therefore, it can conclude that the design of the insulation system is adequate.

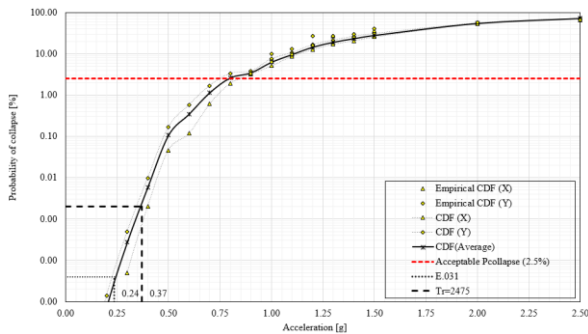


Figure 17 - Cumulative distributions and corresponding fitted collapse fragility functions for shear failure modes of the isolation devices

Finally, Table 5 shown the logarithmic standard deviation (β) for CDF for HDRBs and four-level. The average of β is 0.52. The available P-695 evaluations indicate that, on average, for structures that have been detailed for seismic resistance in the United States The average of β is 0.50 for reinforced concrete SMF ($R=8, \Omega=3$) and reinforced concrete OMF ($R=3, \Omega=3$) (FEMA P695., 2009; Judd and Charney, 2014).

Table 5 - logarithmic standard deviation (β) for isolated building in zone Z4 and soil type S2

Direction	HDRBs	Level				Average
		1	2	3	4	
X	0.47	0.47	0.49	0.53	0.57	0.51
Y	0.57	0.46	0.48	0.54	0.58	0.53

6 CONCLUSIONS

The goal of this study was the evaluation of collapse fragility functions for base-isolated buildings taking into account different sources of aleatory and epistemic uncertainties, and the effect of the horizontal seismic directional demand evaluated through the quotient of the directional ratio (DR) and the spectral bidirectional combination response of two horizontal components (RSDC). In particular, the effects of record-to-record and the model variability have been investigated, for four stories reinforced concrete hospital buildings located in zone 4 (high seismicity) and soil type S2 (shear wave velocities between 350 m/s and 550 m/s). Based on the results of this study, the following conclusions can be drawn:

- a. The factors that allow considering the directionality of the maximum spectral response are 1.30 for structural periods greater than 2.0s and 1.25 for structural periods shorter, based on 40 earthquake events of the Peruvian database, grouped into three types of soil: hard soil, intermediate soil, and soft soil.
- b. The factors for maximum seismic direction according to the Peruvian database are less than those calculated by the FEMA P-695 and the NEHRP adopted by the ASCE SEI 7-5/10 and ASCE SEI 7-5/16.
- c. The factors for maximum seismic direction in the Peruvian territory across the range of periods are similar to those obtained by Huang et al. (2010) for Far-Field and Near-Field in the Western US.
- d. A factor equal to $\beta = 0.52$ for the uncertainty in the collapse capacity was proposed to calculate the acceleration ground motion under the maximum considered earthquake to achieve a targeted collapse probability of 1% in 50 years
- e. The acceptable collapse probability for the maximum earthquake considered is equal to 0.002 for the isolation systems and the maximum acceptable collapse probability for the superstructure is equal to 0.030.
- f. The acceptable collapse probability at maximum earthquake considered for the case of study is much less than the value of 2.5% indicated by the code ASCE SEI7-16. This is due to the low demand for acceleration estimated for periods greater than 2.0s. However, it is important to highlight the importance of estimating the amplification factors by site conditions.

Acknowledgments

The authors wish to express their gratitude to the Civil Engineering Section of the Graduate School of the Pontifical Catholic University of Peru for the realization of this work.

Declarations

Funding

The authors did not receive support from any organization for the submitted work.

Conflicts of interest

The authors have no relevant financial or non-financial interests to disclose.

Availability of data and material

All the processed data has been obtained from the Peruvian database. The information processing has been carried out using calculation tools developed by the authors

Code availability

Not applicable

Authors' contributions

All authors contributed to the study conception and design. Material preparation, data collection and analysis were performed by Arnold Mendo as part of his doctoral thesis. The first draft of the manuscript was written by Arnold Mendo and all authors commented on previous versions of the manuscript. All authors read and approved the final manuscript.

7 REFERENCES

- Abrahamson, N., Gregor, N., Addo, K. (2015). BC Hydro Ground Motion Prediction Equations For Subduction Earthquakes. *Earthquake Spectra*, 32, 150202104017001. doi:10.1193/051712EQS188MR
- Aguilar, Z., Roncal, M., Piedra, R. (2017). Probabilistic Seismic Hazard Assessment in the Peruvian Territory. Paper presented at the 16th World Conference on Earthquake, 16WCEE 2017, Santiago Chile.
- Alva, J. & Castillo, J. (1993). Peligro sísmico en el Perú. Paper presented at the VII Congreso Nacional de Mecánica de Suelos e Ingeniería de Cimentaciones, Lima - Perú.
- Seismic Analysis of Safety-Related Nuclear Structures, (2016).
- Minimum Design Loads for Buildings and Other Structures, (2010).
- Minimum Design Loads and Associated Criteria for Buildings and Other Structures, (2016).
- Atkinson, M. & Boore, M. (2003). Empirical Ground-Motion Relations for Subduction-Zone Earthquakes and Their Application to Cascadia and Other Regions. *Bulletin of the Seismological Society of America*, 93.
- Bakalis, K., & Vamvatsikos, D. (2018). Seismic Fragility Functions via Nonlinear Response History Analysis. 144(10), 04018181. doi:doi:10.1061/(ASCE)ST.1943-541X.0002141
- Baker, J. W. & Cornell, C.A. (2006). Which Spectral Acceleration are you Using? *Earthquake Spectra*, 22(2), 293-312. doi:10.1193/1.2191540
- Bakhshi, A. & Mostafavi, S. (2014). Development of fragility curves for base isolated RC structures. Paper presented at the Proceedings of the 9th International Conference on Structural Dynamics, EUROLYN 2014 Porto, Portugal.

- Beheshti-Aval, S. B., Khojastehfar, E., Zolfaghari, M., Nasrollahzadeh, K. (2014). Collapse fragility curve development using Monte Carlo simulation and artificial neural network. Proceedings of the Institution of Mechanical Engineers Part O Journal of Risk and Reliability, 228. doi:10.1177/1748006X13518524
- Beyer, K. & Bommer, J. (2006). Relationships between Median Values and between Aleatory Variabilities for Different Definitions of the Horizontal Component of Motion. Bulletin of the Seismological Society of America, 97. doi:10.1785/0120050210
- Beyer, K. & Bommer, J. (2007). Selection and Scaling of Real Accelerograms for Bi-Directional Loading: A Review of Current Practice and Code Provisions. Journal of Earthquake Engineering, 11(sup1), 13-45. doi:10.1080/13632460701280013
- Boore, D. M., Watson-Lamprey, J., Abrahamson, N. A. (2006). Orientation-Independent Measures of Ground Motion. Bulletin of the Seismological Society of America, 96(4A), 1502-1511. doi:10.1785/0120050209
- BRIDGESTONE. (2013). Seismic isolation product line-up. In BRIDGESTONE (Ed.).
- Cardone, D., Perrone, G., Plesco, V. (2019). Developing collapse fragility curves for base-isolated buildings. 48(1), 78-102. doi:10.1002/eqe.3126
- Choi, C.-K. (2008). Efficient Monte Carlo simulation procedures in structural uncertainty and reliability analysis-recent advances.
- Clough, R. W. & Penzien, J. (1993). Dynamics of Structures: McGraw-Hill.
- CSI. (2020). SAP2000 Integrated Analysis and Design of Building Systems. In. California, USA: Computers and Structures Inc.
- Damian, N. (2011). Response Spectral Matching of Two Horizontal Ground-Motion Components. JOURNAL OF STRUCTURAL ENGINEERING ASCE.
- Douglas, J. & Gkimpraxis, A. (2017, 2017//). Using targeted risk in seismic design codes: a summary of the state of the art and outstanding. Paper presented at the 6th National Conference on Earthquake Engineering and 2nd National Conference on Earthquake Engineering and Seismology, Bucharest, Romania.
- Douglas, J. & Gkimpraxis, A. (2018, 2018//). Risk Targeting in Seismic Design Codes: The State of the Art, Outstanding Issues and Possible Paths Forward. Paper presented at the Seismic Hazard and Risk Assessment, Cham.
- Ellingwood, B. R. & Kinali, K. (2009). Quantifying and communicating uncertainty in seismic risk assessment. Structural Safety, 31(2), 179-187. doi:https://doi.org/10.1016/j.strusafe.2008.06.001
- EPRI. (2010). Methodology for Developing Seismic Fragilities. Retrieved from California: NEHRP Recommended Provisions: Design Examples FEMA 451, (2006).
- FEMA. (2001). Hazus-MH 2.1 Technical Manual Retrieved from Washington, D: Quantification of Building Seismic Performance Factors, (2009).
- Fernandez-Davila, V.I.. (2007). *Evaluation of the inelastic response of buildings subjected to the two horizontal components of the seismic movement of the ground*. Ph.D.'s thesis. Pontifical Catholic University. Chile.
- Fernandez-Davila, V.I. & Mendo, A. (2020). Damping modification factors for the design of seismic isolation systems in Peru. 0(0), 8755293020926189. doi:10.1177/8755293020926189
- Grant, D. (2004). Modelling and analysis of high-damping rubber bearings for the seismic protection of bridges.
- Grant., D., Fenves., G. L., Whittaker., A. (2004). Bidirectional Modelling Of High-Damping Rubber Bearings. 08(spec01), 161-185. doi:10.1142/s136324690400164x
- Hachem, M. M. (2004). BISPEC: Interactive Software for the Computation of

- Unidirectional and Bidirectional Nonlinear Earthquake Spectra. In *Structures 2004* (pp. 1-12).
- Hassan, W. M. (2020). Assessment of ASCE 7–16 Seismic Isolation Bearing Torsional Displacement. *International Journal of Civil Engineering*, 18(3), 351-366. doi:10.1007/s40999-019-00462-x
- Hong, H. P. & Goda, K. (2007). Orientation-Dependent Ground-Motion Measure for Seismic-Hazard Assessment. *The Bulletin of the Seismological Society of America*, 97, 1525.
- Huang, Y.-N., Whittaker, A. S., Luco, N. (2010). Establishing Maximum Spectral Demand for PerformanceBased Earthquake Engineering: Collaborative Research with the University at Buffalo and the USGS Retrieved from Virginia:
- Huang, Y., Whittaker, A., Luco, N. (2008). Maximum Spectral Demands in the Near-Fault Region. *Earthquake Spectra - EARTHQ SPECTRA*, 24, 319-341. doi:10.1193/1.2830435
- IGP. (2014). Re-evaluación del peligro sísmico probabilístico para el Perú . Retrieved from <http://www.igp.gob.pe/portal>
- Judd, J. P. & Charney, F. A. (2014). Earthquake risk analysis of structures. Paper presented at the Proceedings of the 9th International Conference on Structural Dynamics, Porto, Portugal.
- Kennedy, B. (2015, April, 2015). Overview of Probabilistic Seismic Response Evaluation.
- Kitayama, S. & Constantinou, M.C. (2018). Collapse performance of seismically isolated buildings designed by the procedures of ASCE/SEI 7. *Engineering Structures*, 164, 243-258. doi:<https://doi.org/10.1016/j.engstruct.2018.03.008>
- Kitayama, S. & Constantinou, M.C. (2019). Probabilistic seismic performance assessment of seismically isolated buildings designed by the procedures of ASCE/SEI 7 and other enhanced criteria. *Engineering Structures*, 179, 566-582. doi:<https://doi.org/10.1016/j.engstruct.2018.11.014>
- Kiureghian, A.D. & Ditlevsen, O. (2009). Aleatory or epistemic? Does it matter? *Structural Safety*, 31(2), 105-112. doi:<https://doi.org/10.1016/j.strusafe.2008.06.020>
- Kottke, A. & Rathje, E. (2008). A Semi-Automated Procedure for Selecting and Scaling Recorded Earthquake Motions for Dynamic Analysis. *Earthquake Spectra - EARTHQ SPECTRA*, 24. doi:10.1193/1.2985772
- Luco, N., Bruce, R., Ronald, O., John, D., Jeffrey, K., Charles, A. (2007). Risk-Targeted versus Current Seismic Design Maps for the Conterminous United States. Retrieved from
- Luco, N. & Kircher, A. (2007). Project 07 - Reassessment of Seismic Design Procedures and Development of New Ground Motions for Building Codes. Paper presented at the EERI Seminar on Next Generation Attenuation Models.
- Mansouri, I., Ghodrati Amiri, G., Hu, J. W., Khoshkalam, M., Soori, S., Shahbazi, S. (2017). Seismic Fragility Estimates of LRB Base Isolated Frames Using Performance-Based Design. *Shock and Vibration*, 2017, 5184790. doi:10.1155/2017/5184790
- Mazzoni, S., Hachem, M., Sinclair, M. (2012). An Improved Approach for Ground Motion Suite Selection and Modification for Use in Response History Analysis. Paper presented at the 15th World Conference on Earthquake Engineering, Lisboa.
- McKay, M. D., Beckman, R. J., Conover, W. J. (1979). A Comparison of Three Methods for Selecting Values of Input Variables in the Analysis of Output from a Computer Code. *Technometrics*, 21(2), 239-245. doi:10.2307/1268522
- Mendo, A. (2015). Bases para la implementación de la norma peruana de análisis de diseño de edificios con aislación sísmica. Tesis de Maestría, Pontificia Universidad

- Católica del Perú, Lima.
- Mendo, A. & Fernandez-Davila, V.I. (2016). Desplazamientos de diseño para el sismo máximo probable basados en pseudo-aceleraciones con un objetivo de riesgo en Perú Paper presented at the XVII Jornadas Sudamericanas de Ingeniería Estructural, Paraguay.
- Mendo, A. & Fernandez-Davila, V.I. (2017). Bases for Standard of analysis and design of base isolation system for buildings in Peru. Paper presented at the 16th World Conference on Earthquake, Santiago Chile.
- Mendo, A. & Fernandez-Davila, V.I. (2018). Proposal for the design displacement estimating of seismic isolation system in Peru. Paper presented at the XXXVIII Jornadas Sudamericanas de Ingeniería Estructural, Lima, Peru.
- Montalva, G. A., Bastías, N., & Rodriguez-Marek, A. (2017). Ground-Motion Prediction Equation for the Chilean Subduction Zone. *Bulletin of the Seismological Society of America*, 107(2), 901-911. doi:10.1785/0120160221 %J Bulletin of the Seismological Society of America
- Montuori, G. M., Mele, E., Marrazzo, G., Brandonisio, G., & Luca, A. D. J. B. o. E. E. (2015). Stability issues and pressure shear interaction in elastomeric bearings: the primary role of the secondary shape factor. 14, 569-597.
- Muramatsu, Y., Inoue, K., Katoh, R., Kamitani, N., Sakaguchi, T., Sasaki, Y., . . . Kitamura, H. (2004). Test Results Of Ultimate Properties Of Rubber Bearings For Building (Structures). *AIJ Journal of Technology and Design*, 10(20), 67-70. doi:10.3130/aijt.10.67_2
- Porter, K. (2017). A Beginner's Guide to Fragility, Vulnerability, and Risk. In U. o. C. Boulder (Ed.), (pp. 123). Denver CO, USA: University of Colorado Boulder.
- Rathje, E. M., Abrahamson, N. A., & Bray, J. D. (1998). Simplified Frequency Content Estimates of Earthquake Ground Motions. *Journal of Geotechnical and Geoenvironmental Engineering*.
- Reyes, J. C., Riaño, A. C., Kalkan, E., Quintero, O. A., & Arango, C. M. (2014). Assessment of spectrum matching procedure for nonlinear analysis of symmetric and asymmetric-plan buildings. *Engineering Structures*, 72, 171-181. doi:https://doi.org/10.1016/j.engstruct.2014.04.035
- Sadigh, K., Chang, C. Y., Egan, J. A., Makdisi, F., & Youngs, R. R. (1997). Attenuation Relationships for Shallow Crustal Earthquakes Based on California Strong Motion Data. *Seismological Research Letters*, 68.
- Saez, A., Moroni, M. O., & Sarrazin, M. (2012). Contributions to the Chilean Code for Seismic Design of Buildings with Energy Dissipation Devices. Paper presented at the 15th World Conference on Earthquake Engineering, Lisboa.
- Norma técnica de edificación E.060 Concreto Armado, (2009).
- Norma Técnica E.030 Diseño Sismorresistente, (2016).
- SENCICO. (2017). Aplicativo de peligro sísmico web CPSC. Retrieved from <https://www.sencico.gob.pe/publicaciones.php?id=331>
- Norma técnica E.030 Diseño sismorresistente, (2018).
- Norma Técnica E.031 Aislamiento Sísmico, (2019).
- Sharma, S., & Candia-Gallegos, M. (1992). Seismic hazard analysis of Peru. *Engineering Geology*, 32(1), 73-79. doi:https://doi.org/10.1016/0013-7952(92)90019-U
- Speicher, L., Tinman, M., Quiun, D., & Muñoz, A. (2017). Seismic protection of buildings in Peru using energy dissipation and base isolation. Paper presented at the World Conference on Earthquake, 16WCEE 2017 Santiago Chile.
- Stewart, J. P., Abrahamson, N. A., Atkinson, G. M., Beker, J. W., Boore, D. M., Bozorgnia, Y., . . . Sabol, T. A. (2011). Representation of bidirectional ground motions for

- design spectra in building codes. *Earthquake Spectra*, 27(3), 927-937. doi:10.1193/1.3608001
- Tavera, H. (2017). Actualización del escenario por sismo, tsunami y exposición en la región central del Perú Retrieved from
- Vamvatsikos, D. (2014). Seismic Performance Uncertainty Estimation via IDA with Progressive Accelerogram-Wise Latin Hypercube Sampling. *Journal of structural engineering*, 140. doi:10.1061/(ASCE)ST.1943-541X.0001030
- Vamvatsikos, D., & Cornell, C. (2002). Incremental dynamic analysis. *Earthquake Engineering & Structural Dynamics*, 31(3), 491-514. doi:doi:10.1002/eqe.141
- Vamvatsikos, D., & Cornell, C. A. (2004). Applied Incremental Dynamic Analysis. *Earthquake Spectra*, 20(2), 523-553. doi:10.1193/1.1737737
- Villegas-Lanza, J. C., Chlieh, M., Cavalié, O., Tavera, H., Baby, P., Chire-Chira, J., & Nocquet, J. M. (2016). Active tectonics of Peru: Heterogeneous interseismic coupling along the Nazca megathrust, rigid motion of the Peruvian Sliver, and Subandean shortening accommodation. *Journal of Geophysical Research: Solid Earth*, 121. doi:10.1002/2016JB013080
- Watson-Lamprey, J. (2010). Re: Practical Application of the New ASCE 7-10 Required Procedures for Determining Site Specific Ground Motions
- Watson-Lamprey, J., & Boore, D. (2007). Beyond SaGMRotI: conversion to SaArb, SaSN and SaMaxRot. *Bulletin of The Seismological Society of America - BULL SEISMOL SOC AMER*, 97, 1511-1524. doi:10.1785/0120070007
- Young, R. R., Chiou, S. J., Silva, W. J., & Humphrey, J. R. (1997). Strong Ground Motion Attenuation Relationships for Subduction Zone Earthquakes. *Seismological Research Letters*, 68.
- Zhao, F., Zhang, Y., & Lü, H. (2006). Artificial ground motion compatible with specified ground shaking peaks and target response spectrum. *Earthquake Engineering and Engineering Vibration*, 5(1), 41-48. doi:10.1007/s11803-006-0625-y